Texas A&M University
Mechanical Engineering Department
Turbomachinery Laboratory
Tribology Group

EXPERIMENTAL LEAKAGE AND DYNAMIC FORCED PERFORMANCE OF A GROOVED WET (BUBBLY LIQUID) SEAL

TRC-SEAL-01-18
Research Progress Report to the Turbomachinery Research Consortium

by

Xueliang Lu
Research Assistant

Luis San Andrés
Mast-Childs Chair Professor
Principal Investigator

May 2018

***WET* (BUBBLY) SEALS FOR SUB-SEA MULTIPLE PHASE PUMPS AND *WET* COMPRESSORS**

TRC Project, TEES # 400124-00079

Executive summary

In the subsea O&G industry, multiphase pumps and wet gas compressors are engineered choices as they save O&G transportation and separation facility costs. In these machines, seals handling multiple phase components, must be able to operate without affecting the system efficiency and its dynamic stability. The research in 2018 extends prior work with plain and wavy surface annular seals and presents measurements of leakage and dynamic force coefficients in a grooved seal with diameter D=127 mm, length $L=0.34D$, and clearance c=0.211 mm. The seal has 14 shallow grooves with depth d_g~2.6 c and length L_g~0.034 L.

At a shaft speed 3.5 krpm (23.3 m/s), a mixture of air in ISO VG 10 oil with inlet gas volume fraction (GVF) ranging from 0 (just oil) to 0.7 (mostly air) lubricates the seal. The pressure ratio (inlet/exit) is 2.9, typical for an impeller wear ring seal in an electrical submersible pump. The flow is laminar since the oil is viscous and the pressure drop is low. The measured mixture mass flow rate decreases continuously with an increase in inlet GVF. The seal stiffnesses (direct K and cross coupled k), added mass (M), and direct damping (C) coefficients are constant when the supplied mixture has low gas content, GVF$\leq$ 0.1. As the air volume fraction increases, 0.2 $\leq$ GVF $\leq$ 0.5, the seal direct dynamic stiffness, a function of frequency, becomes nil, whereas k and C reduce steadily. In general, for GVF $\leq$ 0.5, direct damping is invariant with frequency; variations in C occur for GVF =0.7. Compared with a three wave seal (2017), the grooved seal offers much lower force coefficients, in particular damping. Thus, for operation with a low pressure drop as in a wear ring seal, the three wave seal is recommended as it also offers a significant centering stiffness.

Table of Contents

List of tables

List of Figures

Introduction

In the subsea oil and gas industry, multiphase pumping and wet gas compression add pressure to unprocessed fluids thus increasing the tieback distance for oil recovery. The implementation of a multiphase pump could eliminate a topside oil/gas separation station, thus saving up to 30% in CAPEX [1]. One challenge to apply multiphase processing technology is that both pumps and compressors have to work efficiently and reliably with mixtures with a varying gas volume fraction (GVF). For example, a multiphase pump has to process a mixture with GVF varying from 0 to 100%, whereas a *wet* gas compressor must tolerate a gas stream with a liquid volume fraction (LVF) to 5% [1, 2].

In 2014, Bertoneri et al. [4] develop a test stand with a single stage compressor originally designed to process a dry gas. To test whether the compressor could withstand a wet gas condition, the authors inject liquid (water) into the operating compressor. For operation at a maximum speed of 13,500 rpm (shaft surface speed unknown) and with a suction pressure between 10 bara to 18.5 bara, the compressor exhibits a quick increase in rotor lateral vibration as the liquid volume fraction (LVF) suddenly increases to 3% (liquid mass fraction 73%). The authors do not disclose the typical frequency of the rotor vibration.

In the same year, Vannini et al. [5] discuss test results for the rotordynamic performance of the same compressor in Ref. [4]. When installed with a labyrinth seal (as a balance piston), the compressor shows a rotor sub synchronous vibration (SSV) at 0.45X when operating with just 0.5% LVF. After the labyrinth seal (balance piston) is replaced with a pocket damper seal, the amplitude of the SSV reduces from ~20μm to just a few μm. Vannini et al. [6] later use a Computational Fluid Dynamics (CFD) analysis to study the flow field in both a labyrinth seal and a pocket damper seal. The results demonstrate a quick accumulation of liquid in the cavities of the labyrinth seal. Due to centrifugal flow effects, the trapped liquid circulates around the seal circumference with significant momentum. A pocket damper seal (PDS), however, appears not to entrap the liquid.

During the development of a high boost multiphase pump, Bibet et al. [7] test a helicon-axial pump installed with a smooth surface balance piston seal. The pump is targeted to generate a differential pressure of 150 bar, with an inlet GVF up to 60%. For operation with some two-phase flow conditions and with a low differential pressure, the rotor suffers high amplitude SSVs. The authors successfully remove the shaft SSVs after breaking the

long smooth surface balance piston seal into three individual seals and adding swirl breaks into the inlet section of each seal.

Past and ongoing research shows that a two phase flow condition does affect significantly the static and dynamic forced performance of annular seals. Back to 1993, Iwatsubo and Nishino [8] report test results in a pump annular seal (L/D = 1, c/R = 0.014) operating with an air in water mixture. The results show a steady decrease in dynamic force coefficients as the GVF increases, and a random high amplitude rotor lateral vibration occurring for tests with GVF > 0.7.

At the Turbomachinery Laboratory of Texas A&M University, Childs and students [9,10] conduct a series of experiments on annular seals operating with an air in silicon oil (PSF-5cSt) mixture. With a smooth surface seal (L/D=0.75, c/R=0.34%), at a fixed discharge pressure of 6.9 bara and a supply pressure ranging from 27.6 and 48.3 bara, the authors find that the air content in a flowing liquid (LVF=0 to 0.1) can significantly lower the direct stiffness (K) and mass (M) coefficients. A negative K even occurs as the inlet LVF approaches 0.1, thus causing severe rotor sub synchronous vibration. The test evidences a slight increase in direct damping coefficient (C) and cross coupled stiffness (k) as air is mixed into the liquid.

In a separate test program, San Andrés and Lu [11,12,13] (2014 - present) complete extensive experiments to quantify the effect of air on the leakage, shear drag torque, and dynamic force coefficients of various types of annular seals. The experiments are mostly conducted at a shaft speed of 3,500 rpm (ΩR=23.3 m/s) and a low (1.5 bar) supply/discharge pressure difference condition. The inlet GVF spans 0 – 0.9, a typical range for a multiphase pump. The tests with a uniform clearance annular seal show [11] that the leakage and drag torque reduces continuously as the inlet GVF increases to 0.9. Both the seal direct and cross coupled dynamic stiffness become strongly frequency dependent when air is mixed with the liquid stream. The direct damping coefficient (C) is only a function of GVF (decreasing with GVF) and not varying with frequency.

In tests with a three wave seal [12] operating with just a liquid, the seal direct dynamic stiffness K_d=K-$M\omega^2$ reduces with frequency; and K_d increases as the inlet GVF grows to 0.1. K_d remains almost unchanged as the inlet GVF further increases to 0.9. This feature is highly desired as the rise in K_d could push up a pump critical speed and also delay the onset

of system instability to a higher rotor speed. The direct damping (C) and cross coupled dynamic stiffness k_d reduce continuously with GVF. However, the whirl frequency ratio WFR=$C/(\Omega k_d)$ remains relative constant at a magnitude of ~0.47 for operation with either a pure liquid or an air in oil mixture.

Recent tests by San Andrés et al. [13] for two stepped clearance seals (band seals for hydraulic pumps and turbines) demonstrate that the location of the step clearance can lead to very distinct seal dynamic forced performance. For example, when lubricated with a pure liquid, a band seal with the narrow clearance facing the incoming flow produces a significant negative direct stiffness (K) that could cause a static instability [14]. On the contrary, when the narrow clearance is displaced towards the seal exit section, K becomes positive. The mixing of air in both liquid seals causes a recovery of the direct dynamic stiffness K_d. Note that direct air injection into the band seal is sometimes used to stabilize otherwise unstable hydraulic turbines [15,16].

Refs. [11-13] report that seals of various geometries (uniform clearance, wavy-surface, stepped clearance) have distinct force coefficients, and which could lead to differences in the dynamic performance of a turbomachinery. One type of seal whose inner surface is textured with circumferential grooves is commonly used in pumps as wear ring seals [17] and balance drum pistons [18]. In a turbulent flow regime, a grooved seal has a lesser leakage when compared with that in a uniform clearance seal. These seals are expected to show distinct forced performance when operating with a gas-liquid two component flow. However, there is no data showing the performance of such seals operating under a two phase flow condition.

This report continues to assess the effect of a bubbly mixture on the leakage and dynamic force coefficients of a shallow depth grooved seal (d_g/c=2.6), whose dimensions are scaled from a seal in a boiler feed pump. The experiments are conducted at a journal rotational speed of 3.5 krpm (ΩR = 23.3 m/s), supply pressure 2.9 bar (absolute), and an inlet GVF from 0 to 0.7. Dynamic loads exerted on the seal housing with a single frequency (10 Hz - 200 Hz, in steps of 10 Hz) serve to identify the system complex dynamic stiffness matrix (**H**), and from which frequency dependent force coefficients are obtained. The report also details comparisons of mass flow rate and force coefficients between the grooved seal and a three wave seal tested in 2016-2017 [3].

Test rig description

Figure 1 shows schematic views of the grooved seal and a three wave seal (not to scale). Table 1 lists the grooved seal geometry and the fluids physical properties. The grooved seal has length L=43.6 mm and stator diameter D_S=127.42 mm, the shaft diameter D=127 mm, thus the nominal radial clearance is c=½(D_S-D)=0.21 mm. The groove length L_g=1.5 and depth d_g=0.543 mm (14 grooves), and the land length L_l=0.904 mm. Hence the ratio of the groove depth to the radial clearance d_g/c=2.6, a typical magnitude used in various pumps [18].

By contrast, the three wave seal tested in 2016-2017 [3] has a wavy inner surface with maximum clearance c_{max} = 0.274 mm, minimum c_{min} = 0.108 mm, and thus its average clearance c = 0.191 mm. The wavy geometry makes an inherent mechanical preload, thus assisting to generate a large direct stiffness.

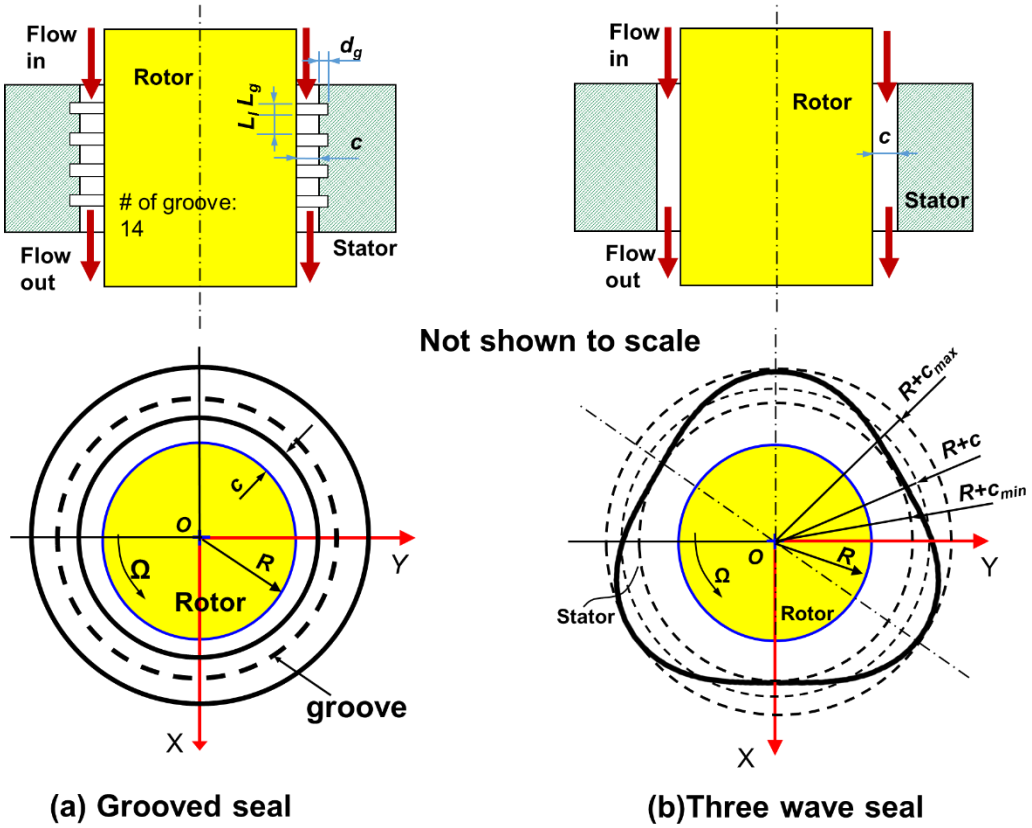

Fig. 1 Schematic views of (a) test grooved seal, and (b) test three wave seal. Grooves seal: c=0.211 mm, L_l=0.904 mm, L_g=1.5 mm, d_g=0.543 mm, number of grooves 14. Three wave seal: c_{max} = 0.274 mm, c_{min} = 0.108 mm, c = 0.191 mm. D=127 mm, L=43.6 mm. (not shown to scale)

Table 1. Dimensions of test grooved seal and fluids physical properties.

Diameter, $D = 2R$	127 mm
Length, L	43.6 mm
Radial clearance c	0.211 mm ± 0.002 mm
Grooved number N_g	14 ± 0.002 mm
Grooved length L_g	1.5 ± 0.002 mm
Grooved depth d_g	0.543 ± 0.002 mm, d_g/c=2.6
Land length L_l	0.904 ± 0.002 mm
ISO VG10 viscosity, μ_l	10.4 cP (at 37 ºC)
Density, ρ_l	830 kg/m^3
Air viscosity, μ_{ga}	0.019 cP (at 37 ºC)
Density, ρ_{ga}	1.14 kg/m^3 at P_a = 1 bara
Max supply & discharge pressures	2.9 bara, 1 bara
Top journal speed, Ω_{max}	3.5 krpm
Rotor surface speed, $\frac{1}{2}D\Omega_{max}$	23.3 m/s

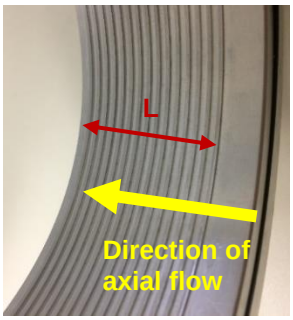

Grooved seal

[1]Figure 2 shows a 3-D view of the seal test rig and the coordinate system (X, Y) for reference of journal motion. The test rig is modified from an earlier seal test rig described in Ref. [3]. Four flexible support rods (90° apart) with a total lateral stiffness K_s and structural damping coefficient C_s connect the seal housing to a massive steel base. Two electromagnetic shakers with a load capacity of 440 N ± 9 N (100 lb$_f$), and installed 90° (X, Y) apart, can excite the seal assembly via two long stingers to produce dynamic motions for the identification of force coefficients. The test rig is designed such that the mass center of the assembled rig is in line with the axis of the (X, Y) stingers along the horizontal plane. During a test, the fluids enter the seal assembly from the top to lubricate the seal, and exit the housing through three holes at the bottom.

[1] The description of the test rig is reproduced from TRC-Seal-01-17 [3]

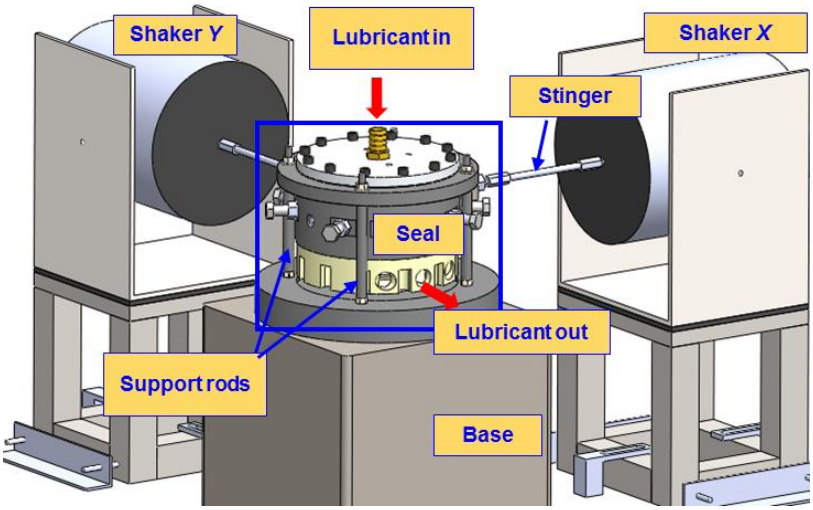

Fig. 2 A graph of the seal test rig with shakers and lubricant supply line

Figure 3(a) shows a cross section view of the seal assembly with lubricant flow path. This arrangement allows to exchange the test seal without disassembly of the entire mechanical structure. The seal element is in installed a housing whose inside diameter (ID) is 3 mm larger than the outside diameter (OD) of the seal, such that the seal can move freely for radial adjustment. Figure 3(b), a view of the cross section A-A, details the seal installation. Four sets (2 bolts as a set) of centering bolts distributed 45˚ apart installed on the seal housing allow radial adjustment of the seal element. During the centering process, a feeler gauge measures the clearance (c) between the journal and the seal. After the seal is centered, a top lid with a bottom surface contacting the top surface of the seal element presses it against the seal housing.

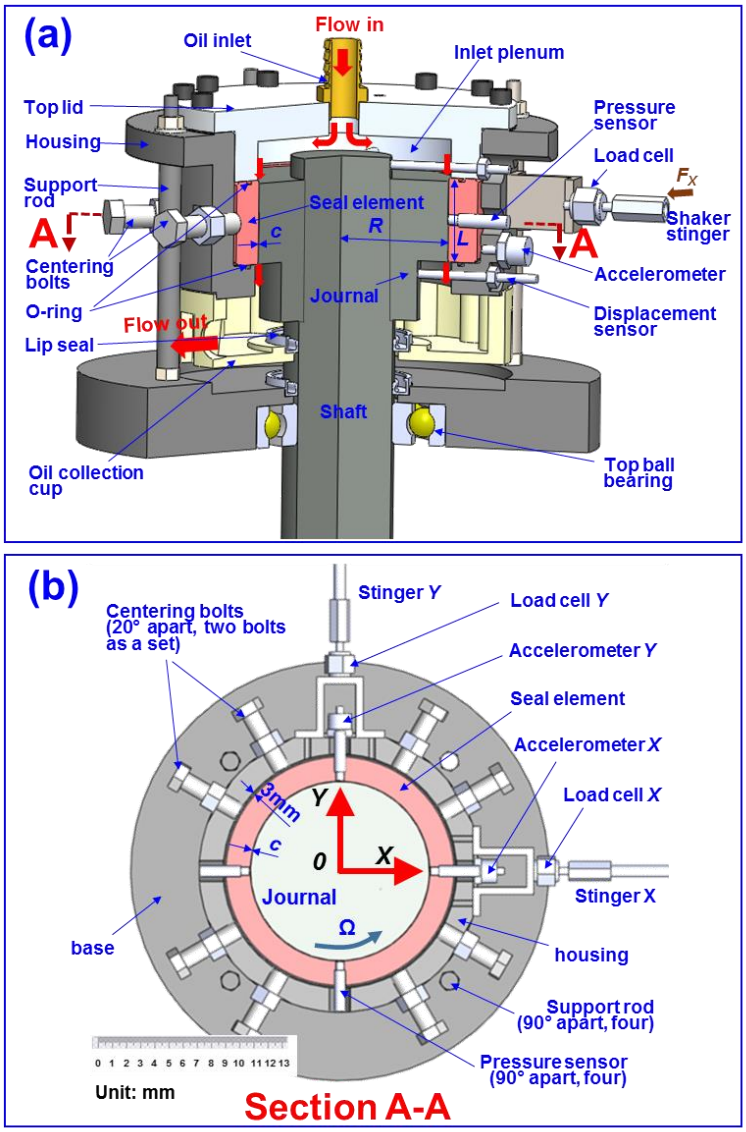

Fig. 3 (a) Cut view of test seal assembly with lubricant flow path, (b) cross section (A-A) view of seal assembly (*L*=43.6 mm, *D*=127 mm, *c* = 0.211 mm).

The arrows in Figure 3(a) depict the lubricant flow path. The fluids enters a plenum on top of the seal housing, and then through the seal annular clearance, to exit into an oil collection cup whose volume is ~3.5 times the size of the inlet plenum. After the seal is lubricated with a mixture, a DC motor, through a transmission belt with a gear ratio of 1.8, drives the shaft supported on two rigid ball bearings (the graph only shows a top ball bearing) to rotate at a maximum speed of 6 krpm.

During the dynamic load tests, two load cells installed on the seal housing record the exerted loads. Four eddy current sensors and two piezoelectric accelerometers record the

ensuing seal housing motions and accelerations. A data acquisition system records voltage signals from sensors at a rate of 12.8 k samples/s and the acquisition time lasts typically 10.24 s. Other instrumentation includes static and dynamic pressure sensors, and flow meters for both the oil and air streams.

Figure 4 shows the fluids circulation system that consist of an air supply line drawing dry air from a large pressurized tank, and a gear pump and oil supply line that delivers ISO VG 10 oil at a constant volumetric flow rate. Two needle valves control the air volumetric flow rate and the oil flow rate. An air mass flow meter measures the air volumetric flow rate (Q_g) at a standard condition (20 ^{o}C and 1 bar(a)), and an oil turbine flow meter records the oil volumetric flow rate (Q_l). Both fluid streams merge into a sparger element with pore size of 2 μm to make an air in oil mixture. By regulating the needle valves, the system operator can make mixtures with any inlet gas volume fraction (GVF = 0 to 1) or liquid volume fraction (LVF = 0 to 1). The inlet GVF is

$$\mathrm{GVF} = \frac{Q_{ga}(P_a / P_s)}{Q_l + Q_{ga}(P_a / P_s)} \tag{1}$$

where Q_{ga} is the air volumetric flow rate at a standard condition (1 bar(a), 20 °C), Q_l is the liquid volumetric flow rate, P_s is the supply pressure, and P_a is the ambient pressure. Accordingly, LVF = (1- GVF). The inlet gas mass fraction (GFM) is

$$\mathrm{GMF} = \frac{\mathrm{GVF} \cdot \rho_{ga} \cdot (P_s / P_a)}{\mathrm{GVF} \cdot \rho_{ga} \cdot (P_s / P_a) + (1 - \mathrm{GVF}) \cdot \rho_l} \tag{2}$$

After passing through the sparger, the mixture flows into the seal assembly to lubricate the seal element, to later exiting the seal housing. The mixture then passes through a bubble eliminator where most of the air bubbles are removed. A gear pump returns the fluids to a large oil reservoir (tank). A division wall divides the oil tank into two parts, such that the mixture (with some remnant air) first returns into the right part of the tank to release the remnant gas. The liquid, having a higher density than the mixture, flows from underneath the division wall to the left part of the tank. This arrangement ensures that the fluid in the left tank is pure oil. A feed pump, whose intake is placed ~ 175 mm below the oil level, delivers the oil into the oil supply line for making the air in oil mixture.

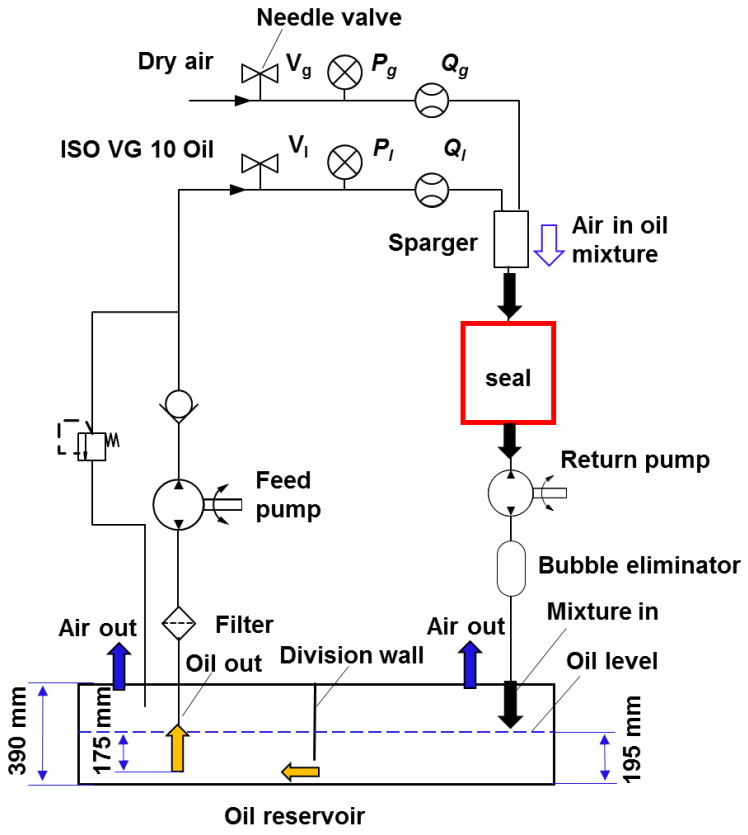

Fig. 4 Air and lubricant circulation flow systems.

At a supply pressure P_s=2.9 ± 0.1 bar(abs) and an inlet temperature T_{in}=37 ± 1 °C, an air in ISO VG 10 oil mixture with inlet gas volume fraction (GVF) varying discretely from 0 to 0.7 feeds the seal. After flowing through the seal film lands, the mixture discharges into ambient pressure P_a=1 bar(a). During the test, the shaft spins at a speed of 3.5 krpm (23.2 m/s).

Recorded flow rate for a shallow depth groove seal

Table 2 lists the recorded seal leakage ($\dot{m}_m$) versus inlet GVF. Compared with a pure liquid condition, the mass flow rate ($\dot{m}_m$) is not affected for operation with a mixture with small inlet GVF (0.03). A further increase in inlet GVF causes a continuous reduction in leakage. Note even though the inlet gas volume (GVF) is as large as 0.7, the gas mass fraction (GMF) is as small as 1%

Fig. 5 shows the normalized leakage ($\dot{\bar{m}}_m$) for the grooved seal and a three wave seal[2] tested in year 2016-2017. The leakage for each seal is normalized with respect to the flow recorded for operation with a pure liquid and a zero shaft speed condition. The measured leakage for both seals decreases steadily with an increase in inlet GVF. Compared with a three wave seal, as the inlet GVF increases, the leakage of the grooved seal reduces faster than that of the three wave seal. Note the grooved seal leaks three times more than the three wave seal because of its larger pressure drop (1.9 bar vs. 1 bar). Hence, the grooves (d_g/c=2.6) effectively reduce the flow resistance at such low Reynolds numbers. For operation with a pure liquid, the grooved seal works in the laminar flow regime as the axial and circumferential Reynolds numbers are just $Re_c = \frac{\rho_l V_c c}{\mu_l} = 392$ and $Re_z = \frac{\dot{m}_{pl}}{\pi D \mu_l} = 54$, respectively.

Table 2 Grooved seal leakage for operation with a pure oil and a mixture. Inlet GVF 0 to 0.7. Supply pressure 2.9 bara, discharge pressure 1 bar(a), shaft speed 3.5 krpm (23.3 m/s).

Inlet GVF (-)	0	0.03	0.10	0.2	0.3	0.5	0.7
GMF (-)	0	$1x10^{-4}$	$5x10^{-4}$	$1.1x10^{-3}$	$1.8x10^{-3}$	$4.3x10^{-3}$	$9.9x10^{-3}$
ρ_m (kg/m^3)	830	805	748	660	578	409	249
$\dot{m}_m$ (g/s)	223±5.1	225±5.5	205±5.1	175±4.6	161±4.9	148±3.3	125±3.1

[2] See TRC-Seal-01-17 [3]. The three wave seal maximum clearance c_{max}=0.274 mm, minimum clearance c_{min}=0.108 mm, mean clearance c=0.191 mm.

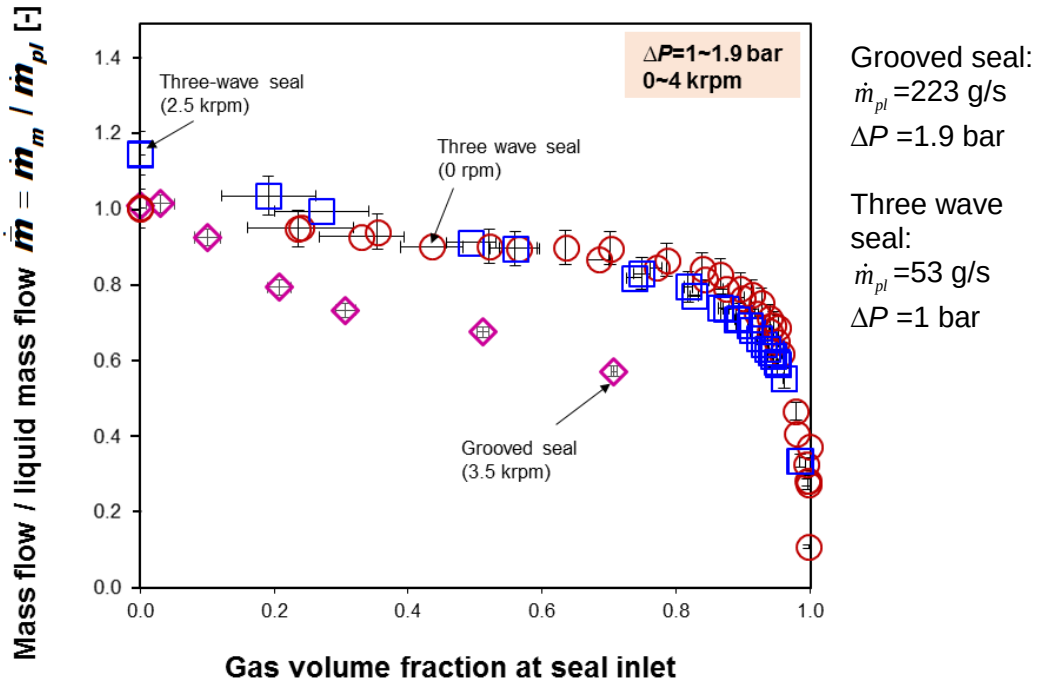

Fig. 5 Normalized leakage ($\bar{\dot{m}}_m$) vs GVF for two seals: a three-wave clearance seal and a grooved seal. Mass flow rate for seal with a pure oil: three-wave seal: c=0.191 mm, $\dot{m}_{pl}$ =53 g/s (ΔP =1 bar, N=0 rpm, T_{in}=39°C); grooved seal: c=0.191 mm, $\dot{m}_{pl}$ =223 g/s (ΔP =1.9 bar, N=3.5 krpm (23.3 m/s), T_{in}=37°C).

Dynamic force coefficients for a shallow depth groove seal

San Andrés and Lu [11] detail a procedure to estimate complex dynamic force coefficients of a mechanical system. The method requires two sets of individual dynamic load tests along two orthogonal directions (X, Y). For example, when the seal is supplied with an oil or a mixture, one shaker applies a periodic load $f_X = f_o e^{i\omega t}$ along the X direction, and the other shaker is at rest. The data acquisition system record the applied forces $\mathbf{F}_{\mathbf{X}(t)} = [f_X = f_o e^{i\omega t}, f_Y = 0]^T$, the ensuing displacement $\mathbf{D}_{\mathbf{X}(t)} = [X_X, Y_X]^T$ with respect to the shaft, and the absolute seal housing acceleration $\mathbf{A}_{\mathbf{X}(t)} = [a_{XX}, a_{YX}]^T$. After the test along the X direction is completed, the test procedure is repeated for the Y direction.

After the test is completed, the time domain data $(\mathbf{F}_{\mathbf{X,Y}}, \mathbf{D}_{\mathbf{X,Y}}, \mathbf{A}_{\mathbf{X,Y}})_{(t)}$ is transformed into the frequency domain to obtain the fundamental component of the Fourier series at each test frequency, i.e., $f_X = f_o\, e^{i\omega t} \rightarrow X_X = \underline{X}_X\, e^{i(\omega t+\phi x)}$ and $Y_X = \underline{Y}_X\, e^{i(\omega t+\phi y)}$, where $i = \sqrt{-1}$ and ϕ_x , ϕ_y are phase angles. Then the matrices for the applied load, the seal housing acceleration, and the displacements are assembled, where $\mathbf{F}_{(\omega)} = [\mathbf{F}_{\mathbf{X}(\omega)} \mid \mathbf{F}_{\mathbf{Y}(\omega)}]$, $\mathbf{A}_{(\omega)} = [\mathbf{A}_{\mathbf{X}(\omega)}$

$| \mathbf{A}_{\mathbf{Y}(\omega)}]$, $\mathbf{D}_{(\omega)} = [\mathbf{D}_{\mathbf{X}(\omega)} | \mathbf{D}_{\mathbf{Y}(\omega)}]$. The entire mechanical system has a complex dynamic stiffness written as

$$\mathbf{H}_{(\omega)system} = \left[\mathbf{F}_{(\omega)} - M_s \mathbf{A}_{(\omega)}\right] \mathbf{D}^{-1}{}_{(\omega)} \tag{3}$$

Subtracting the baseline parameters of the dry system from the lubricated system impedance yields the seal dynamic complex stiffness

$$\mathbf{H}_{(\omega)seal} = \mathbf{H}_{(\omega)system} - \left(\mathbf{K}_s + i\ \omega \mathbf{C}_s\right) \tag{4}$$

Rewrite $\mathbf{H}_{(\omega)seal}$ as

$$\mathbf{H}_{(\omega)seal} = \mathbf{H}^{\shortparallel} + i\ \mathbf{H}^{\perp} \tag{5}$$

where $\mathbf{H}^{\shortparallel}$ is the dynamic stiffness that is in parallel with the displacement, and $\mathbf{H}^{\perp} = \omega \mathbf{C}$ is the quadrature stiffness, perpendicular to the displacement or parallel to the velocity. $\mathbf{K_s}$ = 3.2**I** MN/m, $\mathbf{C_s}$ = 0.38**I** kN-s/m and M_s = 14 kg are the stiffness, damping and mass coefficients obtained from a zero speed condition for the dry system, **I** is a 2x2 identity matrix. Note the uncertainty for the complex dynamic stiffnesses is < 10%.

Figure 6 shows the direct dynamic stiffnesses ($H^{\shortparallel}_{XX}$ and $H^{\shortparallel}_{YY}$) for the grooved seal lubricated with either a pure oil or a mixture with inlet GVF from 0.1 to 0.7. For operation with a mainly oil condition (GVF≤0.1), both $H^{\shortparallel}_{XX}$ and $H^{\shortparallel}_{YY}$ show a quadratic reduction with frequency ω, thus evidencing a frequency independent stiffness (K) and inertia (M) coefficients, that is $H^{\shortparallel} \rightarrow (K - \omega^2 M)$. A least square curve fit for the test data delivers frequency independent stiffness and mass coefficients, as listed in Table 2. In general, when lubricated with a pure liquid, the grooved seal produces small magnitude direct stiffnesses (K_{XX}=0.25 MN/m, K_{YY} =0.34 MN/m) and moderate mass coefficients (M_{XX} =7.2 kg, M_{YY}=6.2 kg). The discrepancy in results between the X and Y directions arises from the identification process. Recall that the test rig has a structure stiffness Ks=3.2 MN/m and an effective mass M_s=14kg. The seal stiffness is just a small fraction (~10%) of the structure stiffness, thus a slight discrepancy in the identified system force coefficients may lead to relative large difference in stiffness.

The experiments include a test for operation with an inlet GVF=0.03; the results being almost identical to those for an inlet GVF=0, and thus not shown for brevity.

For operation with a mixture with inlet GVF=0.2→0.7, $H^{\shortparallel}_{XX}$ and $H^{\shortparallel}_{YY}$ are small in magnitude. Note that the increase in inlet GVF does not change the direct complex dynamic

stiffnesses at a lowest frequency (20 Hz), which indicates that the mixing of gas into the flowing liquid does not promote the generation of a static stiffness.

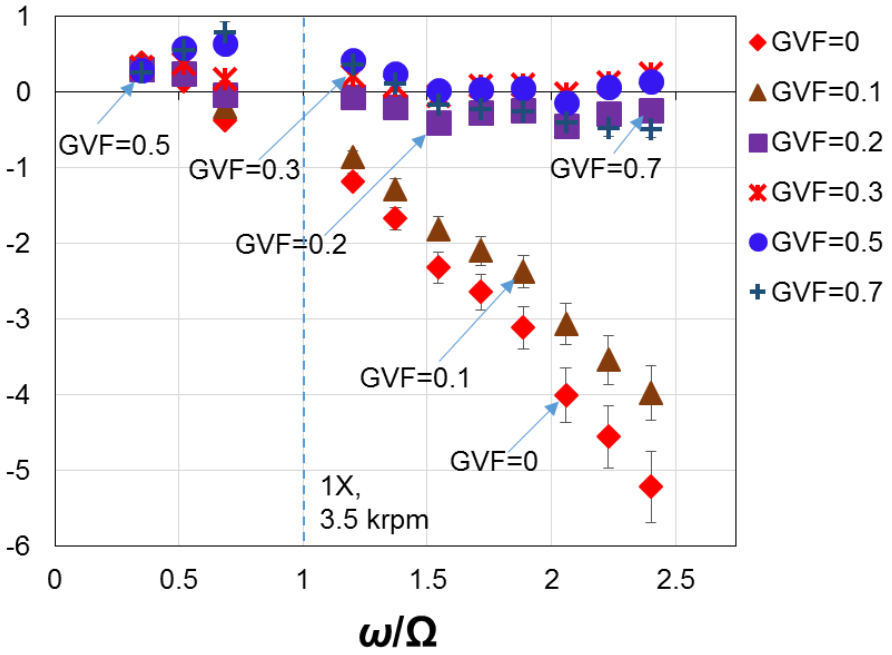

(a) $H^{//}_{XX}$ (MN/m)

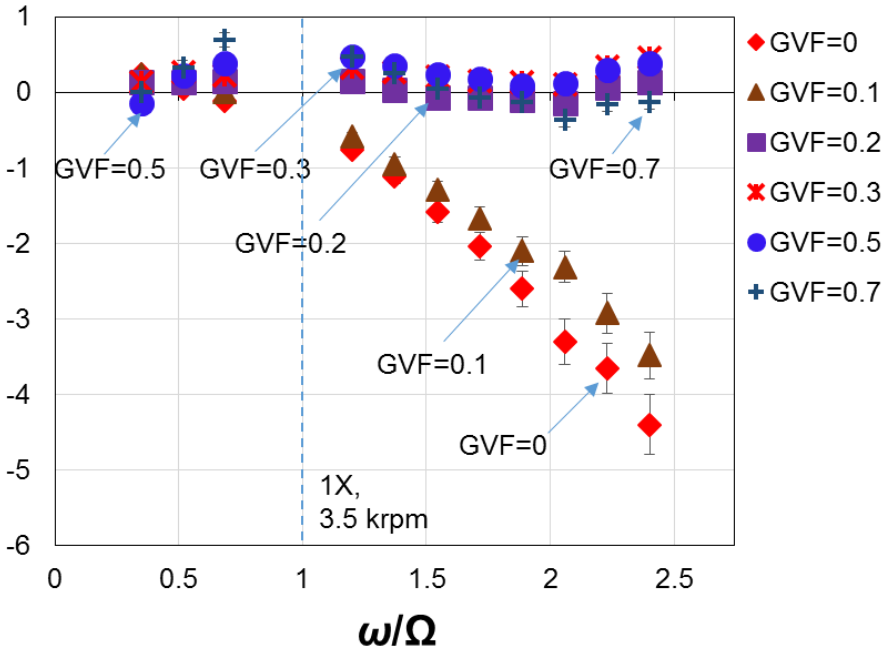

(b) $H^{//}_{YY}$ (MN/m)

Fig. 6 Grooved seal direct dynamic stiffnesses ($H^{//}_{XX}$ and $H^{//}_{YY}$) versus frequency ratio (ω/Ω). Inlet GVF= 0 to 0.7. Supply pressure (P_s) = 2.9 bar(a), ambient pressure (P_a) = 1 bar(a). Journal speed = 3.5 krpm (23.3 m/s).

Figure 7 shows the cross coupled dynamic stiffnesses ($H^{//}_{XY}$ and $-H^{//}_{YX}$) vs. frequency ratio (ω/Ω) for the grooved seal lubricated with either a pure oil or a mixture. The symbols stand for test data and the lines represent the trend of $H^{//}_{XY}$ and $-H^{//}_{YX}$ vs. (ω/Ω) for inlet GVF=0 and 0.7, respectively. For operation with a pure liquid (inlet GVF=0), both $H^{//}_{XY}$ and $-H^{//}_{YX}$ have almost constant magnitude (1.1~1.3 MN/m) over the test frequency range. On the other hand, for operation with a mixture, the cross coupled dynamic stiffnesses increase with frequency and reduce with inlet GVF. $H^{//}_{XY}$ and $-H^{//}_{YX}$ are small in magnitude at (ω/Ω)<1 (GVF=0.3, 0.5 and 0.7).

Figure 8 depicts the quadrature stiffnesses ($H^{\perp}_{XX}$ and $H^{\perp}_{YY}$) vs. frequency ratio (ω/Ω). For operation with either a pure liquid or a mixture with inlet GVF=0→0.5, both $H^{\perp}_{XX}$ and $H^{\perp}_{YY}$ increase linearly with frequency, thus the damping coefficients are constant, i.e., $H^{\perp} \rightarrow \omega C$. However, for operation with a large inlet GVF (0.7), $H^{\perp}_{XX}$ and $H^{\perp}_{YY}$ are nonlinear with frequency. Note that for GVF=0.7, linear curve fits for the quadrature stiffnesses deliver viscous damping coefficients with low correlation coefficients R^2~0.90, 0.87 for C_{XX} and C_{YY}, respectively. As listed in Table 3, the grooved seal shows similar damping coefficients (C_{XX}, C_{YY}) for operation with a pure liquid or a mixture with inlet GVF≤0.2. C_{XX} and C_{YY} reduce quickly as the inlet GVF increases further.

Table 3 Seal frequency independent force coefficients for operation with a pure oil and a mixture. Inlet GVF 0 to 0.7, supply pressure 2.9 bar(a), shaft speed 3.5 krpm.

Inlet GVF	0	0.03	0.10	0.2	0.3	0.5	0.70
K_{XX} (MN/m)	0.25	0.28	0.27	N/A[3]			
K_{YY} (MN/m)	0.34	0.32	0.3				
K_{XY} (MN/m)	1.3	1.2	1.14				
K_{YX} (MN/m)	-1.1	-1	-0.93				
C_{XX} (kN.s/m)	10.4 (0.99)**	10.1 (0.99)	11.0 (0.99)	9.9 (0.99)	8.6 (0.99)	6.6 (0.98)	4.5 (0.9)
C_{YY} (kN.s/m)	9.5 (0.99)	9.4 (0.99)	10.7 (0.98)	9.6 (0.99)	8.1 (0.98)	6.5 (0.97)	4.4 (0.87)
M_{XX} (kg)	7.2	7.2	5.7	N/A			
M_{YY} (kg)	6.2	6.1	4.9				

* The uncertainty for the force coefficients is less than 10%.

** The number in the parenthesis is the R^2 value for a linear curve fit.

[3] N/A means the seal force coefficients are frequency dependent in this particular case.

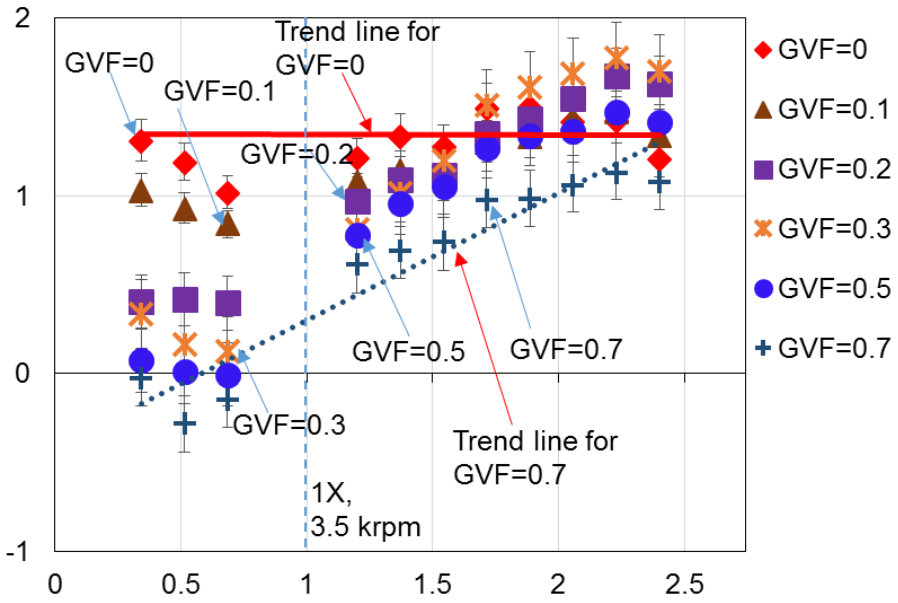

ω/Ω

(a) $H^{//}_{XY}$ (MN/m)

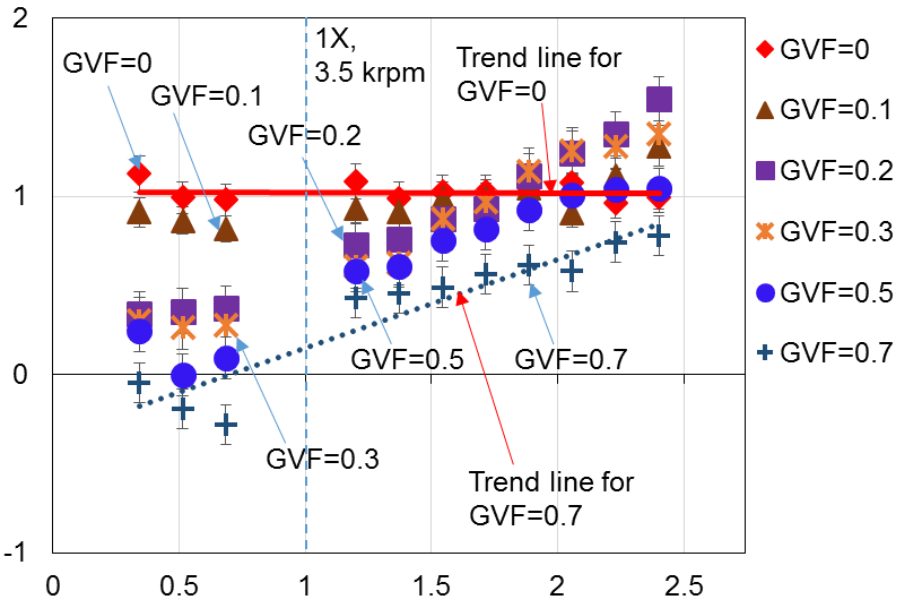

ω/Ω

(b) $-H^{//}_{YX}$ (MN/m)

Fig. 7 Grooved seal cross coupled dynamic stiffnesses ($H^{//}_{XY}$ and $-H^{//}_{YX}$) versus frequency ratio (ω/Ω). Inlet GVF= 0 to 0.7. Supply pressure (P_s) = 2.9 bar(a), ambient pressure (P_a) = 1 bar(a). Journal speed = 3.5 krpm (23.3 m/s). Symbols: test data, lines: trend lines for GVF=0 and 0.7.

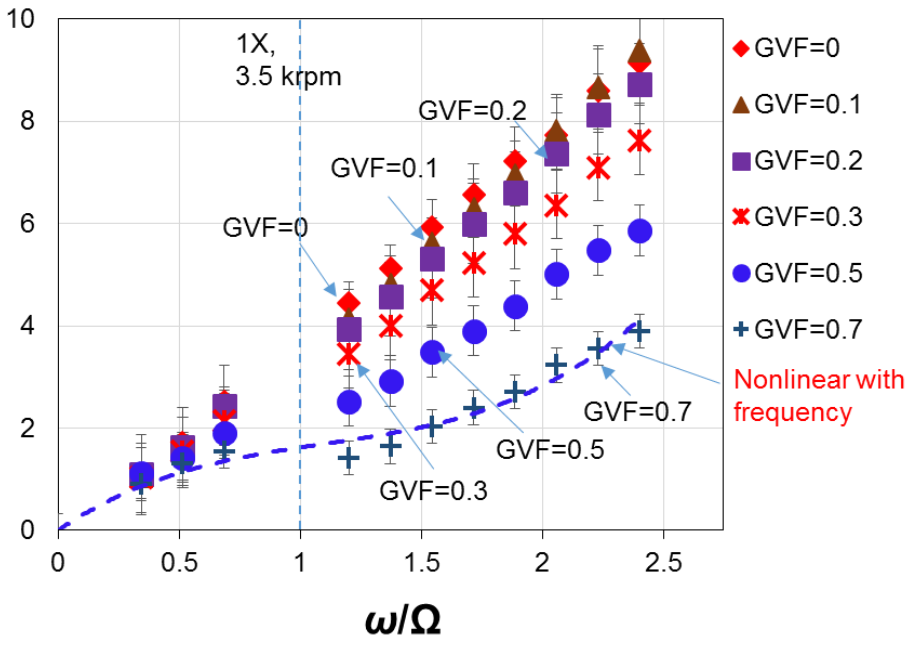

(a) $H_{XX}^{\perp}$ (MN/m)

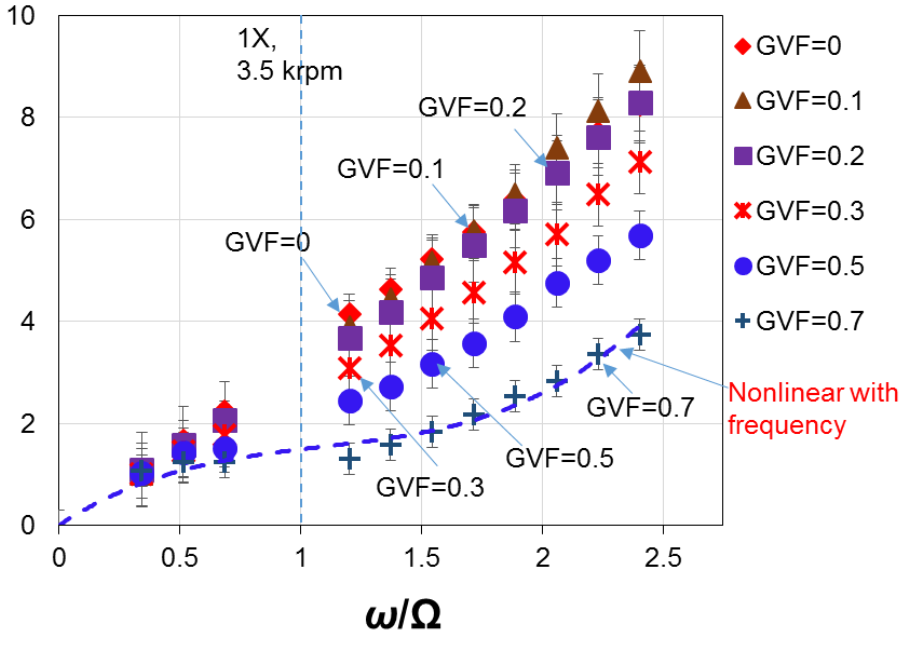

(b) $H_{YY}^{\perp}$ (MN/m)

Fig. 8 Quadrature stiffnesses ($H_{XX}^{\perp}$ and $H_{YY}^{\perp}$) versus frequency ratio (ω/Ω). Inlet GVF= 0 to 0.7. Supply pressure (P_s) = 2.9 bar(a), ambient pressure (P_a) = 1 bar(a). Journal speed = 3.5 krpm (23.3 m/s). Symbols: test data, lines: trend lines for GVF=0 and 0.7.

Figure 9 shows the damping coefficients ($C_{i,j}$, $i,j=X,Y$) versus inlet GVF, where $C_{i,j}$ is obtained from a linear curve fit of $H^{\perp}_{i,j}$, i.e., $C \sim H^{\perp}_{i,j}/\omega$. The direct damping C_{XX} and C_{YY} slightly first increase as the inlet GVF rises from 0 to 0.1; C_{XX} and C_{YY} then show a linear drop as the inlet GVF increases to 0.7. The reduction in direct damping could cause an increase in pump shaft vibrations. Note the cross coupled damping coefficients, C_{XY} and C_{YX}, are relatively small compared with the direct ones. For operation with inlet GVF>0.2, C_{XY} and C_{YX} are negligible, thus not shown on the graph.

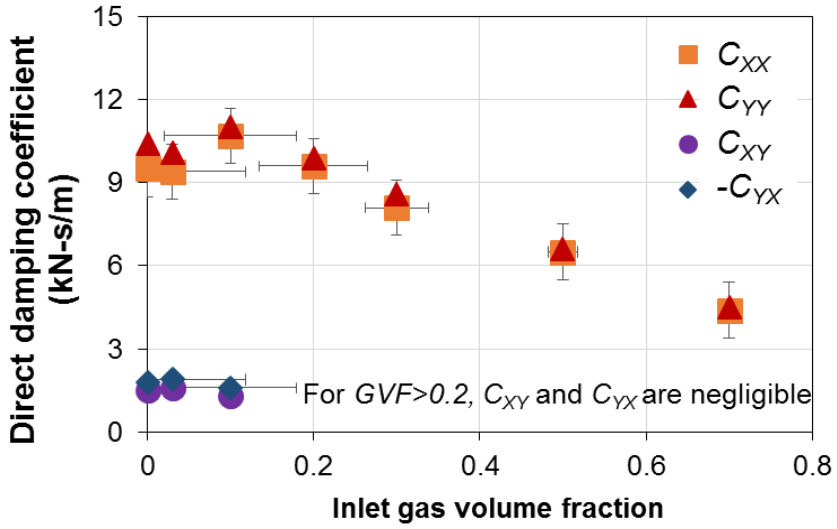

Fig. 9 Direct and cross coupled damping coefficients versus inlet GVF. Inlet GVF= 0 to 0.7. Supply pressure (P_s) = 2.9 bara, ambient pressure P_a = 1 bara. Journal speed= 3.5 krpm (23.3 m/s).

Figure 10 shows the seal effective damping coefficient $C_{eff}=0.5(C_{effXX}+C_{effYY})$ versus frequency for operation with a pure oil and a mixture with inlet GVF as large as 0.7. The error bars denote the variation of C_{eff} between the X and Y directions. Recall

$$C_{effXX} = (H^{\perp}_{XX} - H^{//}_{XY})/\omega,\ C_{effYY} = (H^{\perp}_{YY}+H^{//}_{YX})/\omega \qquad (6)$$

For operation with a pure liquid (GVF=0) and a mixture with inlet GVF = 0.1, C_{eff} increases continuously with frequency. For the test with a pure liquid, C_{eff} approaches zero (the crossover frequency, ω_c) at ~20 Hz. The cross over frequency (ω_c) reduces to a lesser magnitude as inlet GVF = 0.1. Using the force coefficients listed in Table 3, the whirl frequency ratio (WFR=$k/C\Omega$, where $k={}^1/_2(K_{XY}-K_{YX})$ and $C={}^1/_2(C_{XX}+C_{YY})$) can be obtained, as 0.33 and 0.26 for operation with inlet GVF=0 and 0.1, respectively.

For the seal lubricated with a mixture with inlet GVF≥0.2, C_{eff} shows a peculiar peak

at approximately (ω/Ω) = 0.5~0.7. At this time there is no explanation to this phenomenon. Note the increase in inlet GVF causes a continuous reduction to the amplitude of C_{eff}.

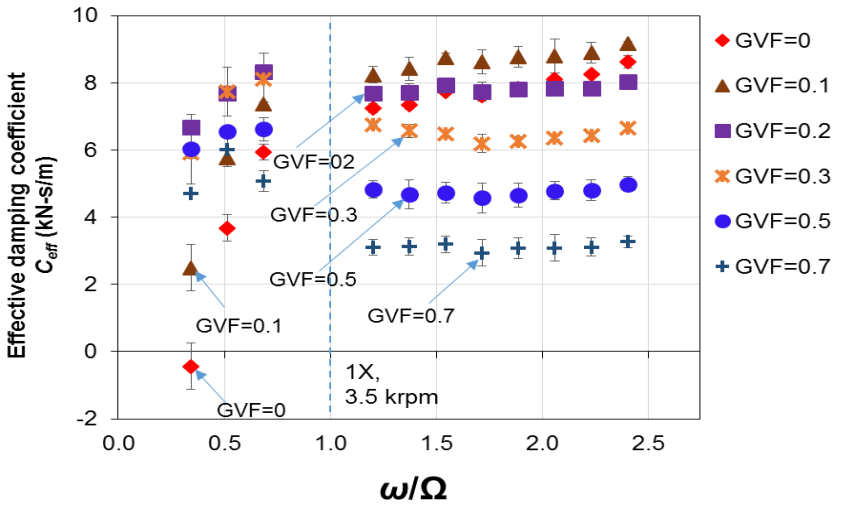

Fig. 10 Effective damping coefficient (C_{eff}) versus frequency ratio (ω/Ω). Inlet GVF= 0 to 0.7. Supply pressure (P_s) = 2.9 bar(a), ambient pressure (P_a) = 1 bar(a). Journal speed = 3.5 krpm (58.3 Hz).

Comparison of dynamic force coefficients between grooved seal and a three wave seal

Figures 11 to 14 show the experimental force coefficients for the grooved seal (current tests) and the three wave seal (c=0.191 mm) tested in 2016-2017 [3]. The tests for the grooved seal are conducted with a mixture with inlet GVF = 0, 0.2, 0.7 and supplied at pressure P_s = 2.9 bara. The three wave seal is tested under similar conditions with inlet GVF=0, 0.2, 0.8, and a supply pressure P_s = 2.5 bara. The shaft speed = 3.5 krpm (ΩR = 23.3 m/s) in the experiments for both seals. For better comparison, the data shown is the arithmetic average coefficients along the X and Y directions, i.e., $H_D^{//} = ½(H_{XX}^{//} + H_{YY}^{//})$ and $H_C^{//} = ½(H_{XY}^{//} - H_{YX}^{//})$. The vertical error bars denote the variability of the coefficients along the X and Y directions.

For both seals, Figure 11 shows the direct dynamic stiffness $H_D^{//}$ vs. frequency ratio (ω/Ω). For operation with a pure liquid, the dynamic stiffness of both seals decreases in a parabolic form versus frequency. The grooved seal generates a smaller dynamic stiffness than the three wave seal. For operation with an air in oil mixture (GVF>0.2), the dynamic stiffness of the grooved seal is negligible in magnitude compared with that of the three wave seal.

Figure 12 shows the cross coupled dynamic stiffnesses $H_C^{//}$ vs. frequency ratio (ω/Ω). For operation with either a pure liquid or a mixture, the grooved seal generates a lesser cross coupled stiffness than the three wave seal does. In Figure 13, the direct damping coefficient for the grooved seal is just ~30% of that in the three wave seal. Note for both seals operating with inlet GVF=0.7, 0.8, C reduces with frequency.

Figure 14 shows the effective damping coefficients (C_{eff}) vs. frequency ratio (ω/Ω). For all test conditions, the three-wave seal always shows a larger C_{eff} than the groove seal when $\omega > \omega_c$, where ω_c is the cross-over frequency at which $C_{eff} = 0$. For a pure liquid condition, the whirl frequency ratio (WFR) of the grooved seal and the three wave seal are 0.33 and 0.47, respectively.

The test results reveal that the grooved seal generates a lesser direct dynamic stiffness and a smaller effective damping than a three wave seal does. The grooved seal has a lower whirl frequency ratio than a three wave seal.

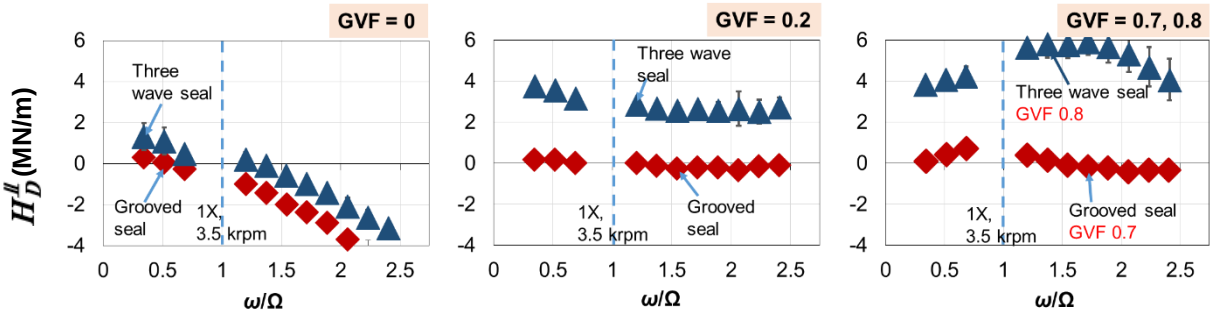

Fig. 11 Grooved seal and three-wave seal: direct dynamic stiffness ($H_D^{//}$) vs. frequency ratio (ω/Ω). Inlet GVF: 0, 0.2, 0.7, 0.8. Shaft speed: 3.5 krpm (23.3 m/s). Supply pressure (P_s): 2.5 bara (three wave seal), 2.9 bara (grooved seal).

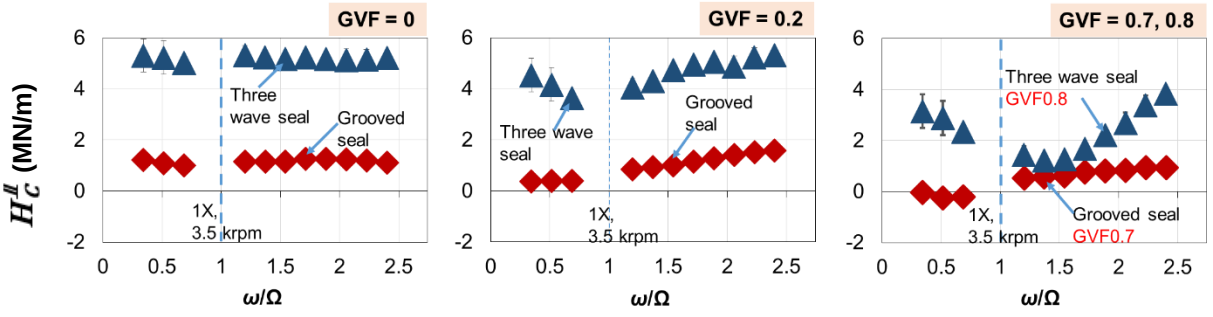

Fig. 12 Grooved seal and three-wave seal: cross coupled dynamic stiffness ($H_C^{//}$) vs. frequency ratio (ω/Ω). Inlet GVF: 0, 0.2, 0.7, 0.8. Shaft speed: 3.5 krpm (23.3 m/s). Supply pressure (P_s): 2.5 bara (three wave seal), 2.9 bara (grooved seal).

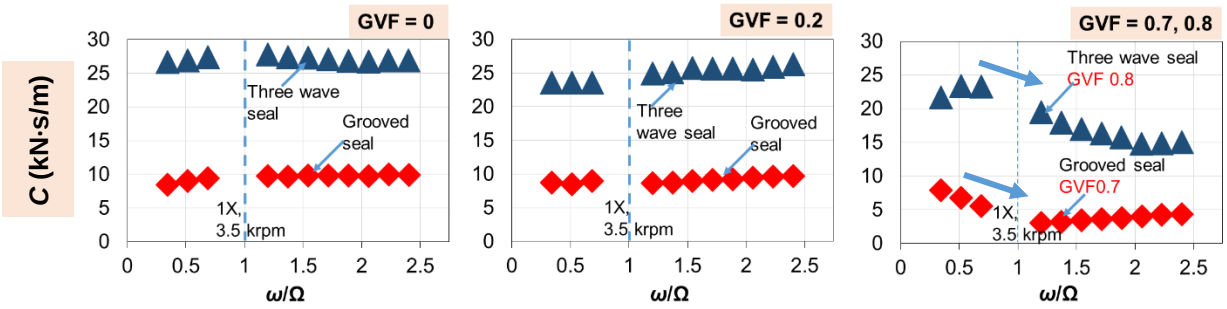

Fig. 13 Grooved seal and three-wave seal: direct damping (*C*) vs. frequency ratio (*ω*/Ω). Inlet GVF: 0, 0.2, 0.7, 0.8. Shaft speed: 3.5 krpm (23.3 m/s). Supply pressure (P_s): 2.5 bara (three wave seal), 2.9 bara (grooved seal).

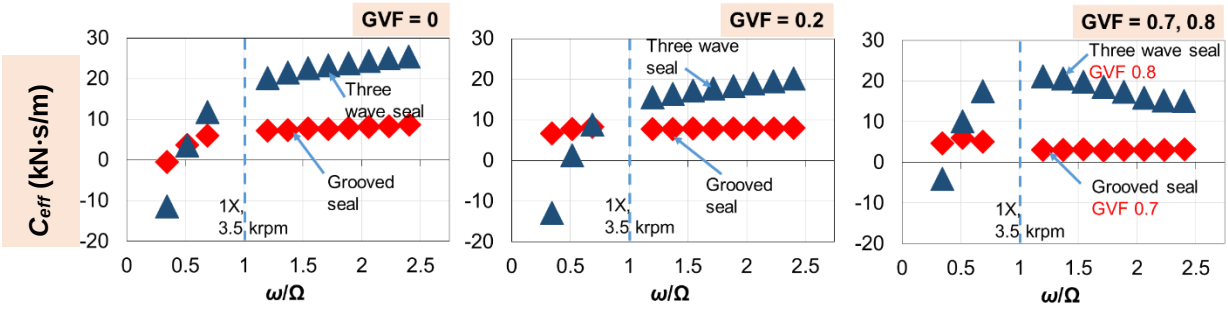

Fig. 14 Grooved seal and three-wave seal: effective damping (C_{eff}) vs. frequency ratio (*ω*/Ω). Inlet GVF: 0, 0.2, 0.7, 0.8. Shaft speed: 3.5 krpm (23.3 m/s). Supply pressure (P_s): 2.5 bara (three wave seal), 2.9 bara (grooved seal).

Conclusion

Grooved seals are commonly used as wear ring seals and balance drum pistons in pumps. These seals show a distinct static and dynamic forced performance when operating with a gas-liquid two component flow.

This report shows force coefficients of a shallow depth grooved seal operating at a shaft speed of 3.5 krpm (23.3 m/s). An air in oil mixture with an inlet GVF = 0 to 0.7 lubricates the seal at a supply pressure 2.9 bar(a). Single frequency dynamic load tests assist to deliver force coefficients. The analysis of the test results leads to the following conclusions:

1. In the laminar flow regime (Re_c=392, Re_z=54), the grooved seal leaks more than the three wave seal. As the inlet GVF increases, the (normalized) leakage of the grooved seal reduces faster than that of a three wave seal [3].
2. A small amount of gas (GVF~0.03) in the oil does not affect the force coefficients of the test grooved seal.

3. For operation with a mixture with inlet GVF≤ 0.1, the seal shows frequency independent force coefficients (*K*, *k*, *C* and *M*).
4. For operation with a mixture with inlet $0.2 \leq \text{GVF} \leq 0.5$, the direct dynamic stiffness of the grooved seal is negligible. The cross coupled dynamic stiffness coefficients reduce with an increase in the inlet GVF.
5. The grooved seal shows frequency independent damping coefficients (*C*) for operation with either a pure liquid or an air in oil mixture ($\text{GVF} \leq 0.5$). *C* increases about 8% as the inlet GVF increases from 0 to 0.1, and then decreases monotonically as the inlet GVF further increases. For operation with a mixture with a large inlet GVF (0.7) the direct damping coefficients reduce with frequency. The cross coupled damping coefficients are a minute fraction of the direct damping coefficients.
6. Compared with a three wave seal with a similar average clearance, the grooved seal offers much smaller force coefficients, in particular the damping coefficients (*C*). However, the grooved seal shows a whirl frequency ratio of 0.33, a smaller magnitude than that of the three wave seal at 0.47.
7. Under a low supply pressure condition (P_s-P_a=1.9 bar), the flow in both the test grooved seal and a test three wave seal is laminar. The grooved seal leaks more and offers lower stiffness compared with those of the three wave seal. Thus, the three wave seal is best recommended than a grooved seal for operation under a low pressure drop condition.

Thus far, the experiments show that a grooved seal is not a good option to reduce leakage for operation in the laminar flow; the grooves greatly reduce the flow resistance. Some tests conducted by San Andrés et al. [13] demonstrate that a band clearance seal with a narrow clearance facing the incoming flow is more efficient on restricting leakage, but this seal creates a large negative stiffness. Future work will focus on using direct air injection into a band clearance seal to increase its static stability and to control its leakage.

Acknowledgements

The authors thank the interest and financial support provided by the Texas A&M University Turbomachinery Research Consortium. Thanks to Ph.D. cantidate Mr. Tingcheng Wu for assisting to test the grooved seal.

Nomenclature

c	Seal radial clearance [m]
c_{max}, C_{min}	maximum and minimum clearance of three-wave seal [m]
$C_{i,j}$	$C_{i,j}=H^{\perp}_{ij}/\omega$, Seal damping coefficient [N.s/m], $i, j = X, Y$
C_{eff}	$C_{eff}=(H^{\perp}_{XX} - H^{//}_{XY})/\omega$, effective damping coefficients [N.s/m], $i, j = X, Y$
D	$D = 2R$, Journal diameter [m]
d_g, L_g, L_l	Groove depth and length, land length [m]
F_X, F_Y	Components of external excitation force [N]
H	$H=H^{//} + i\, H^{\perp}$, Seal complex dynamic stiffness [N/m]
$H^{//}_D$, $H^{//}_C$	$H^{//}_D = ½(H^{//}_{XX} + H^{//}_{YY})$, $H^{//}_C = ½(H^{//}_{XY} - H^{//}_{YX})$, Seal average dynamic stiffness [N/m]
$H^{//}_{i,j}$	Seal dynamic stiffnesses [N/m], $i, j = X, Y$
$H^{\perp}_{i,j}$	ωC_{ij}. Seal quadrature stiffness [N/m], $i, j = X, Y$
K	Seal direct static stiffness [N/m]
K_d	$K_d=K-M\omega^2$, Seal direct dynamic coefficients [N/m]
k_d	Seal cross coupled dynamic coefficients [N/m]
L	Seal length [mm]
$\dot{m}_l, \dot{m}_g$	Mass flow rate for pure liquid and pure gas [kg/s]
$\dot{m}_m$	$\dot{m}_m = \dot{m}_l + \dot{m}_g$, Mass flow rate of air in oil mixture [kg/s]
$M_{i,j}$	Seal mass coefficients [N.s/m], $i, j = X, Y$
N	Shaft rotational speed [rev/min]
P_a, P_s	Ambient pressure and supply pressure [Pa]
Q_l , Q_g	Flow rate for pure liquid and pure gas [m^3/s]
Q_m	Flow rate for two-phase mixture [m^3/s]
Re_c , Re_z	$Re_c = \frac{\rho_l V_c c}{\mu_l}$, and $Re_z = \frac{\dot{m}_{pl}}{\pi D \mu_l}$, flow circumferential and axial Reynolds numbers
T	Torque [N·m]
V_c	Bulk flow circumferential velocity
X,Y	Seal cartridge displacements [m]
μ_l, μ_{ga}	Liquid and gas viscosities at ambient pressure and T = 37ºC [Pa.s]
ρ_l, ρ_{ga}	Liquid and gas densities at ambient pressure and T = 37ºC [kg/m^3]
ρ_m	Mixture or two-phase fluid density [kg/m^3]
Ω	N x(π/30). Shaft angular speed [rad/s]
ω	Excitation frequency [Hz]

Matrices and vectors

A	Absolute acceleration vector [m/s^2]
C	Damping matrix, $\mathbf{C = C_S + C_{seal}}$ [N·s/m]
$\mathbf{C_S}$	$\mathbf{C_S} = 3.8 \cdot 10^2$ N·s/m **I**, Structure damping coefficient
D	Seal cartridge displacement vector [m]
F	External excitation force vector [N]
H	**K-** ω^2 **M** + $i\,\omega$ **C.** System complex dynamic stiffness matrix [N/m]
I	2x2 identity matrix.

$\mathbf{K}$	System stiffness matrix, $\mathbf{K} = \mathbf{K_S} + \mathbf{K_{seal}}$ [N/m]
$\mathbf{K_S}$	$\mathbf{K_S}=3.2\cdot10^6$ N/m **I**, Structure stiffness coefficient
$\mathbf{M_S}$	$\mathbf{M_S}$=14 kg **I**, Structure mass coefficient

Abbreviations

GVF	Gas volume fraction
GMF	Gas mass fraction
LVF	Liquid volume fraction
OD	Outside diameter of the shaft
ID	Inside diameter of the seal
SSV	Sub-synchronous vibration
WFR	Whirl frequency ratio

Subscripts

m	Mixture or two component flow
g, l, pl	Gas, liquid, pure liquid
S	Structure

References

[1] Gong, H., Falcone, G., et al., 2012, "Comparison of Multiphase Pumping Technologies for Subsea and Downhole Applications," Oil and Gas Facilities, **1**(01), pp. 36-46.

[2] Brenne, L., Bjorge, T., and Gilarranz, J., 2005, "Performance evaluation of a Centrifugal Compressor Operating under Wet Gas Conditions," *Proc. 34th Turbomachinery Symposium*, Houston, TX, September 12-15.

[3] Lu, X., San Andrés, L., 2017, "Leakage and Rotordynamic Force Coefficients of a Three-wave (Air in Oil) Wet Annular Seal," TRC-Seal-01-17, Annual Progress Report to the Turbomachinery Research Consortium, Texas A&M University, May.

[4] Bertoneri, M., Wilcox, M., Toni, L. and Beck, G., 2014, "Development of Test Stand for Measuring Aerodynamic, Erosion, and Rotordynamic Performance of a Centrifugal Compressor under Wet Gas Conditions," *Proc. of ASME Turbo Expo 2014*, Düsseldorf, Germany. ASME Paper No. GT2014-25349.

[5] Vannini, G., Bertoneri, M., Del Vescovo, G. and Wilcox, M., 2014, "Centrifugal Compressor Rotordynamics in Wet Gas Conditions," *Proc.* 43rd *Turbomachinery & 30th Pump Users Symposium*, Houston, TX, September 23-25.

[6] Vannini, G., Bertoneri, M., Nielsen, K.K., Ludiciani, P., and Stronach, R., 2016, "Experimental Results and Computational Fluid Dynamics Simulations of Labyrinth and Pocket Damper Seals for Wet Gas Compression," ASME J. Eng. Gas Turb. Power, **138**, p. 052501.

[7] Bibet, P. J., Klepsvik, K. H., Lumpkin, V. A., and Grimstad, H., 2013, "Design and Verification Testing of a New Balance Piston for High Boost Multiphase Pumps,"

Proc. 29th International Pump User Symposium, Houston, TX, October 1-3.

[8] Iwatsubo, T., and Nishino, T., 1993, "An Experimental Study on the Static and Dynamic Characteristics of Pump Annular Seals," *Proc. of the 7th Workshop on Rotordynamic Instability Problems in High Performance Turbomachinery*, College Station, TX, May 10–12, pp. 30-45. https://ntrs.nasa.gov/archive/nasa/casi.ntrs.nasa.gov/19940029673.pdf.

[9] Zhang, M., Mclean, J., Jr., and Childs, D., 2017 "Experimental Study of the Static and Dynamic Characteristics of a Long Smooth Seal with Two-Phase, Mainly-Air Mixtures," ASME J. Eng. Gas Turbine Power, **139**(12), p. 122504.

[10] Tran, D. L., 2017, "Experimental Study of The Static and Dynamic Characteristics of a Long (L/D=0.75) Smooth Annular Seal Operating under Two-Phase (Liquid/Gas) Conditions with Three Inlet Preswirl Configurations," M.S. thesis, Texas A&M University.

[11] San Andrés, L., and Lu, X., 2018, "Leakage, Drag Power and Rotordynamic Force Coefficients of an Air in Oil (Wet) Annular Seal," ASME J. Eng. Gas Turb. Power, **140**, p. 012505.

[12] Lu, X., and San Andrés, L., 2018, "Leakage and Rotordynamic Force Coefficients of a Three-wave (Air in Oil) Wet Annular Seal: Measurements and Predictions," ASME Paper No. GT2018-75200.

[13] San Andrés, L., Lu, X., and Zhu, J., 2018, "On the Leakage and Rotordynamic Force Coefficients of Pump Annular Seals Operating with Air/Oil Mixtures: Measurements and Predictions," *Proc. 2nd TAMU Asia Turbomachinery & Pump Symposium*, Singapore, March 12-15.

[14] Nishimura, H., Horiguchi, H., Suzuki, T., Sugiyama, K., and Tsujimoto, Y., 2016, "Sub- and Super-Synchronous Self-Excited Vibrations of a Columnar Rotor Due to Axial Clearance Flow," *28th IAHR Symposium on Hydraulic Machinery and Systems*, Grenoble, France, July 4-8.

[15] Ruud, F.O., 1976, "Vibration of Deriaz Pumps at Dos Amigos Pumping Plant," ASME J. Fluids Eng., December, **98**(4), pp. 674-679.

[16] Smith, D.R., Price, S.M., and Kunz, F.K., 1996, "Centrifugal Pump Vibration Caused by Supersynchronous Shaft Instability Use of Pumpout Vanes to Increase Pump Shaft Stability," *Proc. 13th International Pump Users Symposium*, Houston, TX, March 5-7.

[17] Nordmann, R., Dietzen, F. J., Janson, W., Frei, A., and Florjancic, S., 1986, "Rotordynamic Coefficients and Leakage Flow of Parallel Grooved Seals and Smooth Seals," *Proc. of the 5th Workshop on Rotordynamic Instability Problems in High-Performance Turbomachinery*, College Station, TX, June 2-4, pp. 129–153. https://ntrs.nasa.gov/archive/nasa/casi.ntrs.nasa.gov/19870012766.pdf.

[18] San Andrés, L., Wu, T., and Maeda, H., Tomoki, O., 2018, "A Computational Fluid Dynamics Modified Bulk Flow Analysis for Circumferentially Shallow Grooved Liquid Seals," ASME J. Eng. Gas Turb. Power, **140**(1), p. 012504.